Thermochimica Acta 480 (2008) 53–60

Contents lists available at ScienceDirect

Thermochimica Acta

journal homepage: www.elsevier.com/locate/tca

Reactivity of ethylene oxide in contact with basic contaminants

Linh T.T. Dinh, William J. Rogers, M. Sam Mannan*

Mary Kay O'Connor Process Safety Center, Artie McFerrin Department of Chemical Engineering, Texas A&M University System, MS-3122 College Station, TX 77843-3122, USA

ARTICLE INFO

Article history:
Received 30 May 2008
Received in revised form
16 September 2008
Accepted 21 September 2008
Available online 30 September 2008

Keywords:
Reactivity
Ethylene oxide
Alkali-contaminants
Adiabatic calorimetry

ABSTRACT

The reactivity of ethylene oxide (EO) with contaminants such as potassium hydroxide (KOH), sodium hydroxide (NaOH), and ammonium hydroxide (NH_4OH) was measured in this work using the automatic pressure tracking adiabatic calorimeter (APTAC). Each contaminant was investigated using three different concentration levels of around 0.10 g, 0.50 g, and 1.0 g in roughly 14 g EO. The research results show that KOH, NaOH, and NH_4OH have significant effects on EO thermal stability. Reductions of onset temperatures were measured as the contaminant concentrations were increased. NH_4OH caused the highest reactivity compared to the other contaminants. KOH is a contaminant that reduced the onset temperature of pure EO to near room temperature even at a low concentration. The key exotherm parameters and profiles that are critical to the design and operation of safer chemical plant processes are also provided in detail.

1. Introduction

Ethylene oxide (EO) has the molecular formula of H_2COCH_2. It is the simplest of the cyclic ethers and very reactive because of its strained ring (see Fig. 1). Its reactions proceed mainly via ring opening and are highly exothermic.

EO is a colorless gas at room temperature and atmospheric pressure. The liquid has a characteristic of ether-like odor. Some important physical properties of EO is shown in Table 1.

EO is highly flammable and poses a dangerous fire and explosion risk. Pure EO with a flash point of −18 °C can be ignited without air or oxygen [1]. Under appropriate conditions, EO is known to undergo a variety of reactions, such as isomerization, polymerization, hydrolysis, combustion, and decomposition, which produces considerable energy.

Despite the hazards, EO is still a major industrial chemical. Its annual worldwide production is 11 million tons [1] and is among the top 3% of high volume chemicals produced in the United States [2]. EO is widely used in the production of many important surfactants, solvents, and specialty chemicals [1].

Due to its very reactive behavior and wide industrial applications, EO has been involved in a number of serious incidents resulting in major damage as well as fatalities [1–8]. Contamination is a main cause of EO incidents.

Among the contaminants, alkalis have the relatively high possibility in contacting with EO due to their indispensable role in many processes and plants involving EO. For instance, many of the ethoxylation reactions use an alkali metal hydroxide, especially potassium, or sodium hydroxide, as a basic catalyst.

In the presence of trace impurities such as alkalis, EO thermal stability may reduce, causing unexpected runaway reactions even at normal conditions. Many past incidents in which alkali-contaminants were in contact with EO for unintentional reasons occurred and created hazardous situations. For example, an incident occurred during the ethoxylation of glycerine. The local concentrations of alkali arising from the thermal decomposition of potassium soaps presented as an impurity in the sucroglyceride. The generated alkali may have initiated exothermic polymerization of the oxide [6,7]. Another ethoxylation reactor exploded because the potassium hydroxide (KOH) catalyzed a reaction of the EO in the vapor space of the reactor, which increased the temperature in localized areas of the reactor head to the decomposition temperature [1,6].

Despite many incidents, only a few studies have investigated the reactivity of EO in contact with contaminants. Published investigations were for iron oxides, water, and sodium hydroxide solution [9–12]. No research on the contamination by KOH or NH_4OH has been reported. This work included research on the reactivity of EO in the presence of KOH, (anhydrous) NaOH, and ammonium hydroxide (NH_4OH). Although the sodium hydroxide (NaOH) solution contamination has been studied [12], research on anhydrous NaOH contamination provides insights on the effect of NaOH compound alone, while the study with

* Corresponding author. Tel: +1 979 862 3985; fax: +1 979 458 1493.
E-mail address: mannan@tamu.edu (M. Sam Mannan).

0040-6031/$ – see front matter © 2008 Elsevier B.V. All rights reserved.
doi:10.1016/j.tca.2008.09.013

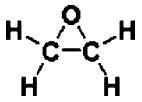

Fig. 1. The structural formula of EO.

Table 1
Some important physical properties of EO.

Property	SI units
Molecular weight	44.1 g mol^{-1}
Melting point	161.46 K
Boiling point	283.6 K
Flammability limits	3–100 vol.%
Auto ignition temperature	702 K

NaOH solution observed the combined effects of NaOH and water.

2. Experimental

2.1. Samples

Lecture bottle cylinders with 227 g EO (99 + % EO from Aldrich, catalog No. 38,761-4) supplied EO for all experiments. Samples were used as received with no additional purification or treatment processes.

For experiments reported in this work, KOH 90% from Mallinckrodt (catalog number 6984-04) was used. NaOH 99% was from Mallinckrodt (catalog number 7708-10) and NH_4OH 30% from Baker (catalog number 9721-01) was used.

In each test, EO samples of 14.01 ± 0.03 g were brought into contact with one of the contaminants at amounts of 0.10 ± 0.01 g, 0.50 ± 0.02 g, or 1.0 ± 0.02 g, while the weight of the titanium cells were 32.49 ± 2.06 g.

2.2. Apparatus

All of the experiments were performed using an automatic pressure tracking adiabatic calorimeter (APTAC). A summary of APTAC test conditions is presented in Table 2.

Due to the gaseous nature and toxicity of EO, the normal procedure for external sample loading to the APTAC cell was not applicable, so a special apparatus configuration was designed. Fig. 2 illustrates the equipment used to transfer and measure the weight of the EO sample.

2.3. Procedure

In this work, each contaminant was investigated with three amounts of roughly 0.10 g, 0.50 g, and 1.0 g contaminant in contact with around 14 g EO. Each combination was carried out three times for repeatability evaluation and deviation calculations.

All experiments were performed in a closed cell environment without air inside the APTAC cell. A heat-wait-search mode (HWS) of operation was applied for all of the runs. For this mode, the sample was heated to an initial search temperature and the temperature was allowed to stabilize in 25 min. Steps of 10 °C were conducted at a rate of 4 °C/min. The system changed to search mode to detect an exotherm thereafter (25 min more). An exothermic activity was detected when a threshold of self-heating rate of 0.1 °C/min was exceeded, and the APTAC followed the reaction adiabatically until the sample was depleted or one of shutdown criteria was satisfied. If no exothermic activity was detected within the search mode, the sample was heated to the next search temperature and the procedure was repeated.

Because of EO hazard characteristics, the experimental procedures were performed carefully. First, cleaning is performed to remove contaminants from the test cell and tubing. Flushing of the test cell and transfer line with acetone was performed several times. Then, the system was dried by flowing compressed nitrogen gas for 5 min. An amount of roughly 0.10 g, 0.50 g, or 1.0 g of one of the three selected contaminants was loaded into the sample cell before attaching the sample cell containing the contaminant to the top of the containment vessel. Next, a series of purging and evacuation cycles was applied to reduce the amount of oxygen in the test cell and transfer line. After evacuation, the sample vessel was kept under a vacuum of about 6.90–20.7 kPa and submerged in a dry-ice acetone bath to cool the test cell to −78 °C to allow EO loading at a good rate. By doing this, ethylene oxide vapors from the lecture bottle were transferred and condensed in the test cell. The loaded amount was monitored by the weigh scale under the EO lecture bottle. Valves 2 and 3 were closed to stop transferring EO when the scale indicated that 14 g EO was loaded. The dry-ice acetone mixture was removed. Finally, the APTAC containment vessel was closed and locked before running an experiment. The whole loading arrangement can be shown in Fig. 2.

Generally, for testing NH_4OH, there were no significant differences in the experiment procedure for each contaminant except for the preparation steps of the NH_4OH. This contaminant, which has very high vapor pressure, was kept at very low temperature (roughly −70 °C) during the oxygen removal cycles to prevent its loss.

2.4. Phi-factor

In the APTAC, a thin-wall 2.5 in titanium sample cell was employed to limit the amount of heat which the cell absorbs from the sample. The ratio of the total heat of reaction to the heat absorbed by the sample in the laboratory instrument, or the relative thermal capacitance of the cell plus sample to the sample alone is represented by the phi-factor, Φ [13,14]:

$$\Phi = 1 + \frac{m_c C_c}{m_s C_s}$$

where m_c (g) is the sample vessel mass, C_c (J g^{-1} K^{-1}) is the sample vessel specific heat, m_s (g) is the sample mass and C_s (J g^{-1} K^{-1}) is the sample specific heat.

The phi-factor has the effect of dampening the thermal magnitude of a real system. The relative wall thermal capacitance might

Table 2
Summary of the APTAC test conditions.

Temperature and pressure	Value	Other settings	Value
Start temperature (°C)	20–100	Heat mode: heat-wait-search	
Final search temperature (°C)	250	Exotherm threshold (°C/min)	0.1
Temperature increment (°C)	10	Exotherm limit (°C)	300
Cool-down temperature (°C)	50	Heat rate (°C/min)	4
Temperature shutdown (°C)	500	Heat rate shutdown (°C/min)	400
Pressure shutdown (kPa)	13100	Pressure rate shutdown (kPa/min)	68,947

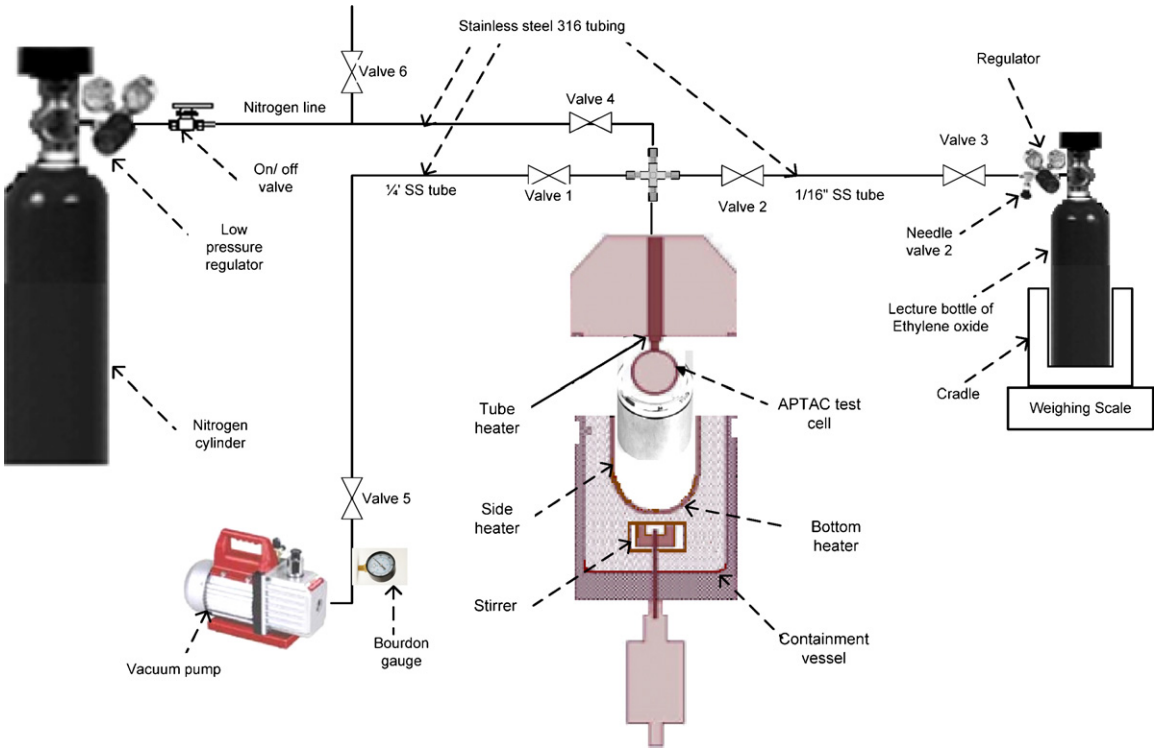

Fig. 2. Schematic of transferring EO into APTAC cell.

be very small in the case of large-scale equipment such as an industrial reactor. Hence, phi-factor is an important issue for scaling laboratory results to industrial processes, where Φ factors typically are low (i.e. close to 1, the minimum value).

In this work, the phi-factor cannot be measured directly by the APTAC and was calculated using the equation above. The EO average heat capacity of 2.0 J g^{-1} K^{-1} used in the phi-factor calculation was derived from the literature over the range of 300–1000 K [15]. The average heat capacity of titanium [16] was estimated to be 0.57 J g^{-1} K^{-1}. In these experiments, the phi-factor ranges between 1.59 and 1.65.

3. Results and discussion

3.1. Pure ethylene oxide

In order to successfully understand the reactivity of EO with the contaminant or the contaminant effects on pure EO, it is necessary to know the pure ethylene oxide behavior in the absence of contaminants. The reactivity of pure EO investigated using the APTAC exhibited considerable exothermic activity. As can be seen in Fig. 2, pure EO reached an onset temperature of around 200 °C, which is in good agreement to the results of the previous research [9,11] (Fig. 3).

The corresponding pressure–time relationship and self-heat rate behavior of pure EO appear in Figs. 4 and 5, respectively.

3.2. Ethylene oxide in contact with potassium hydroxide

Three experimental mixtures with different contaminant amounts (0.1 g, 0.5 g, and 1.0 g KOH) and 14 g EO were conducted (0.70, 3.53, and 7.07% weight contaminant). Fig. 6 depicts the sample temperature–time curves. For an amount of only 0.1 g KOH, an exotherm begins at approximately 50 °C, which is much lower than the onset temperature of pure EO at roughly 200 °C. For 0.5 g

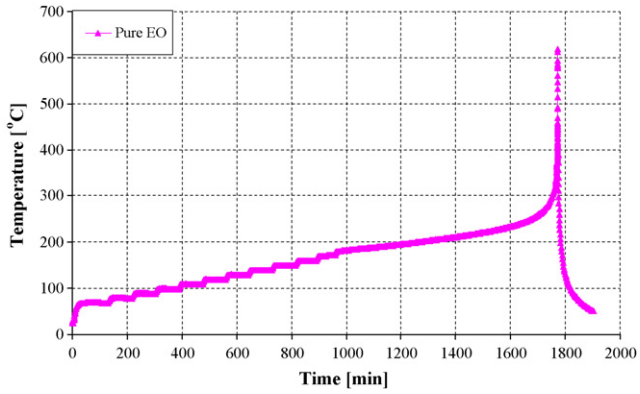

Fig. 3. Temperature history of pure EO in the APTAC.

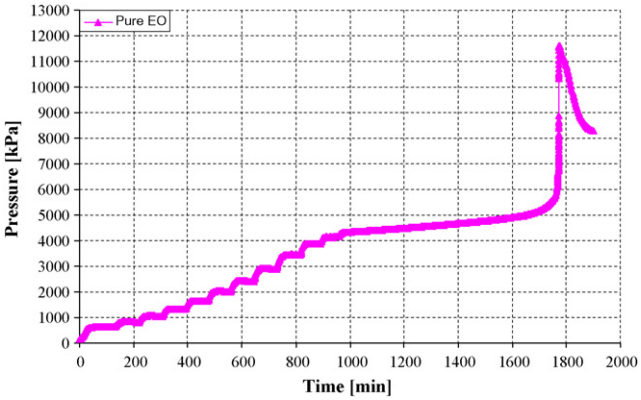

Fig. 4. Pressure history of pure EO in the APTAC.

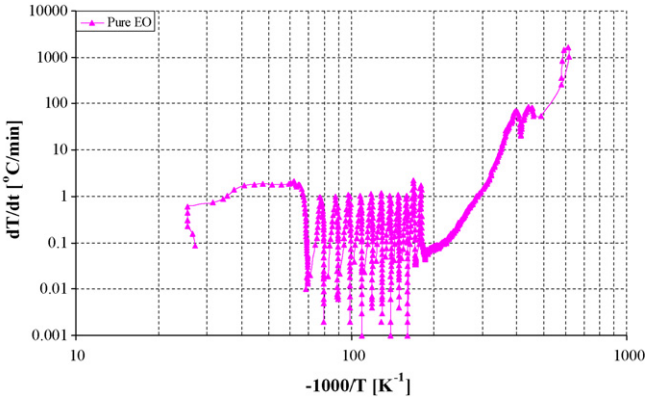

Fig. 5. Self-heat rate profiles of pure EO in the APTAC.

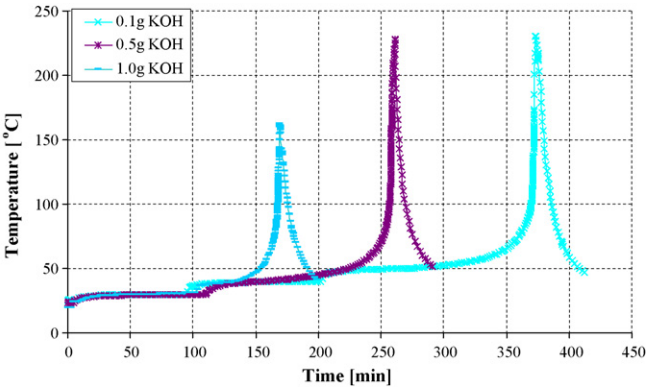

Fig. 6. Temperature history of EO/KOH samples.

and 1.0 g KOH, an exotherm appeared at around 30 °C, near the minimum starting temperature of the APTAC. The onset temperature decreased with increasing KOH concentration. This figure also shows that the mixture inside the cell eventually reached a maximum temperature of around 160 °C, 230 °C, or 240 °C for KOH masses of 1.0 g, 0.5 g, and 0.1 g KOH, respectively. As can be seen in Fig. 6, as KOH concentration decreases the maximum temperature attainable from the runaway increases.

Fig. 7 shows the pressure variation as a function of time. As can be seen in Fig. 7, the pressure rises sharply and reaches roughly 3792 kPa for the case of 0.1 g KOH. The maximum pressure decreased as the concentration of the KOH was increased.

The measured heat rates with respect to temperatures are displayed in Fig. 8. In this figure, it can be seen that the more the

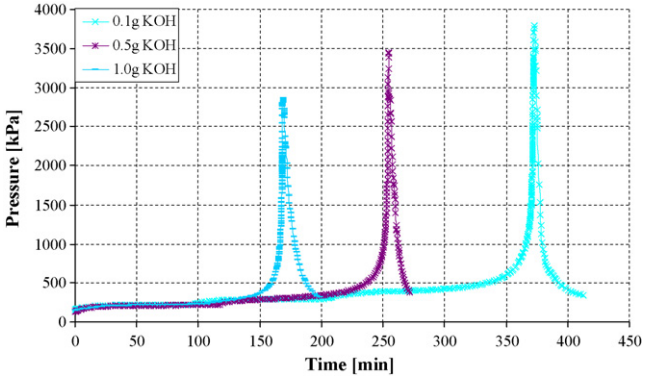

Fig. 7. Pressure history of EO/KOH samples.

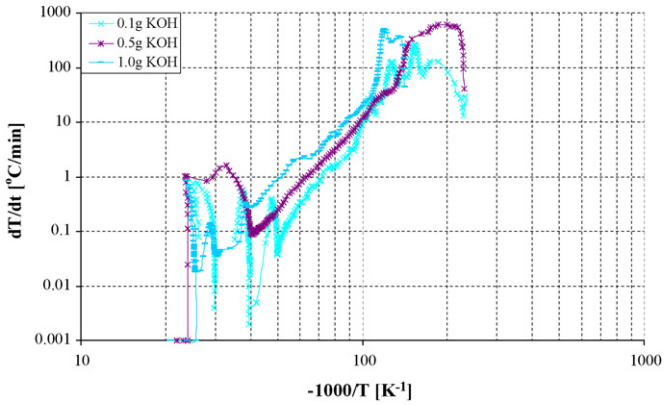

Fig. 8. Self-heat rate–temperature profiles of EO/KOH.

contaminant KOH added, the sooner the exotherm of the sample starts.

For different combinations, parallel trends are exhibited in the pressurization rate versus temperature plots in Fig. 9. Although the maximum pressure attained by each run was different, there was no significant difference observed among the maximum pressurization rates in the investigated range of contaminant concentrations.

The pressure–temperature curves (see Fig. 10) indicate the presence of the vapor as well as non-condensable gases in the cell. The curves are divided into three main parts:

(1) From A to B, the mixture was heated by the surroundings and the exothermic reaction energy. As can be seen in Fig. 10, the observed curves follow the ones during EO heating.

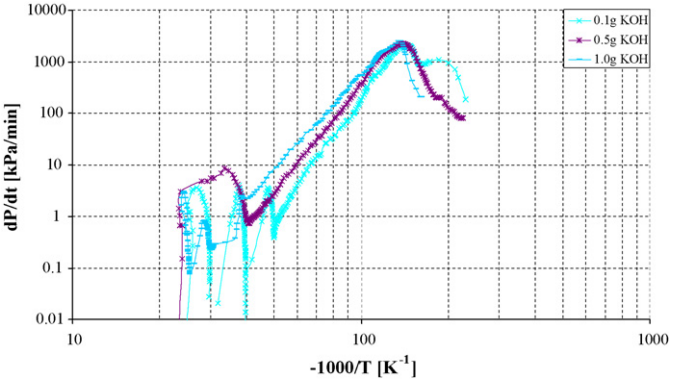

Fig. 9. Pressurization rate profiles of EO/KOH samples.

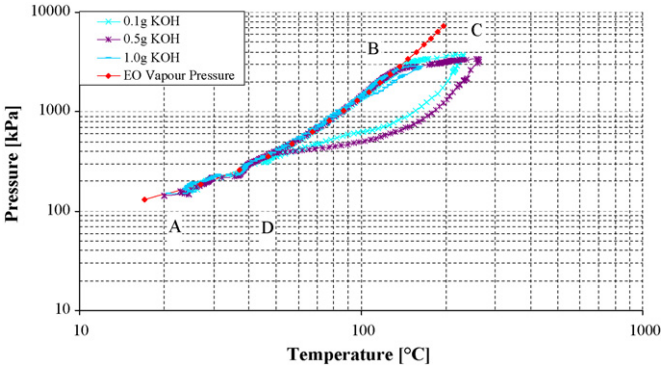

Fig. 10. Pressure–temperature profiles of EO/KOH samples.

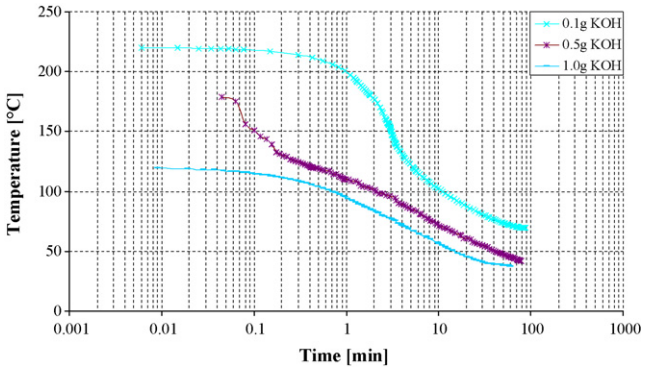

Fig. 11. Time-to-maximum rate profiles of EO/KOH samples.

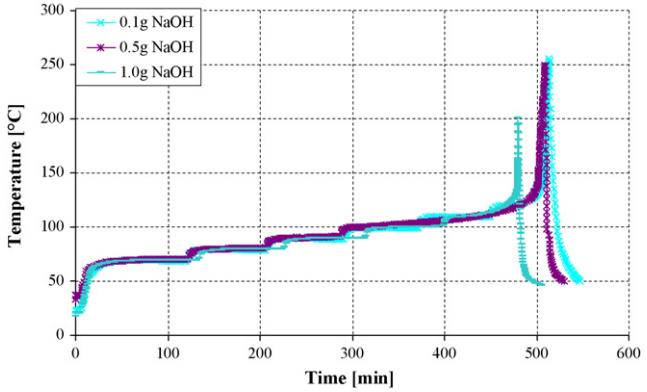

Fig. 12. Temperature history of EO/NaOH samples.

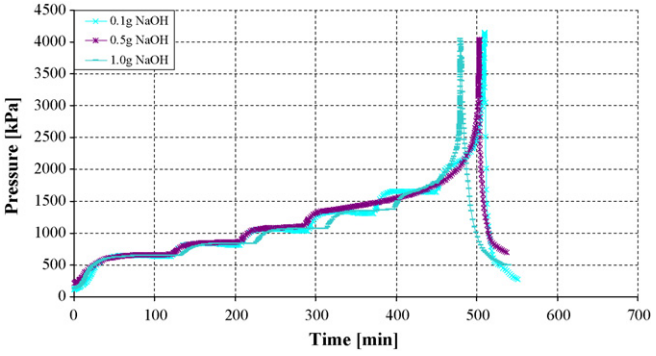

Fig. 13. Pressure history of EO/NaOH samples.

(2) From B to C, the exothermic reactions strongly released heat and increased the mixture temperature, while the pressure did not increase because of ethylene oxide consumption. Thus, the pressures from these tests fall away from the EO vapor pressure curves and the slopes of their curves were lower than those of the curves from A to B.
(3) During cool-down (from C to D), both pressure and temperature decreased due to a shutdown of the APTAC heaters. The observed pressure and temperature curves were not straight lines because some products condensed during this period. The fact that the cooling curve slopes were lower than the heating curve slopes indicates that EO was converted into less volatile components which can be the products of polymerization reactions in the presence of KOH [12].

The rapidity of the ethylene oxide exothermic activity in the presence of KOH is illustrated by the time-to-maximum rate plot of Fig. 11. In the case of 1.0 g KOH, beginning near ambient temperature the EO exothermic reaction rate would reach its maximum rate in about 60 min, but by 60 °C, the time to maximum rate was only about 10 min. For the smaller amounts of KOH, more time is needed for the heat rate to reach its maximum.

A summary of important parameters in the experimental results with contaminant KOH is presented in Table 3. As can be seen in Table 3, when the contaminant concentration was increased from 0.1 g, the onset temperatures, maximum temperature rates, maximum pressure rates resulted in higher values indicating increased, although the observed maximum temperatures and maximum pressures were lower.

3.3. Ethylene oxide in contact with sodium hydroxide

The reactivity of EO in contact with the contaminant sodium hydroxide was measured for three levels: 0.1 g, 0.5 g, and 1.0 g NaOH. Fig. 12 depicts the curves of measured sample temperatures with respect to time. For the NaOH contamination, EO self-heating rates of 0.1°/min or greater occurred at onset temperatures of 105 °C or above. As the NaOH concentration increased, the average onset temperature slightly decreased. The maximum temperatures with NaOH were within 200–250 °C. Similar trends were observed in pressure–time behavior (see Fig. 13), which paralleled trends observed for the temperature versus time plots.

Fig. 14 illustrates the observed self-heat rate profiles for EO/NaOH mixtures. Self-heat rates of over 0.1 °C/min were observed at temperatures above 100 °C, which was much higher than the ones observed for the KOH. Acceleration to the average self-heat values of 1401, 679, and 526 °C/min were obtained for the 0.1 g, 0.5 g, and 1.0 g amounts, respectively. Based on Fig. 13, EO exotherms with lower NaOH concentrations exhibited slightly greater maximum self-heat rates. The plots of pressurization rate versus temperature are also displayed in Fig. 15.

The pressure versus temperature plots are shown in Fig. 16. The plot for the case of 0.1 g NaOH exhibited the same behavior as described for the EO/KOH mixtures that generated the condens-

Table 3
APTAC experimental results for EO/KOH, EO/NaOH, and EO/NH_4OH mixtures.

Contaminant	Φ	T_{on} (°C)	T_{max} (°C)	P_{max} (kPa)	dT/dt_{max} (°C/min)	dP/dt_{max} (kPa/min)	T_{MR} (min)
0.1 g KOH	1.65	52–62	233–247	3826–4102	243–334	1337–1944	74–102
0.5 g KOH	1.62	38–42	221–241	3081–3468	590–650	1958–2757	75–81
1.0 g KOH	1.61	31–37	155–169	2757–3006	529–625	2461–2847	55–61
0.1 g NaOH	1.64	115–125	223–255	4116–4143	1386–1416	2364–3026	53–77
0.5 g NaOH	1.62	105–111	217–249	4019–4171	639–719	2316–2716	60–64
1.0 g NaOH	1.60	103–107	188–212	3840–4102	480–572	2213–2737	52–60
0.1 g NH_4OH	1.64	156–160	562–580	11727–12389	3154–3288	25131–26262	148–306
0.5 g NH_4OH	1.62	57–61	526–534	11941–12369	1249–1357	83061–113370	78–126
1.0 g NH_4OH	1.59	20–22	138–166	2509–2868	575–635	7646–8059	162–200

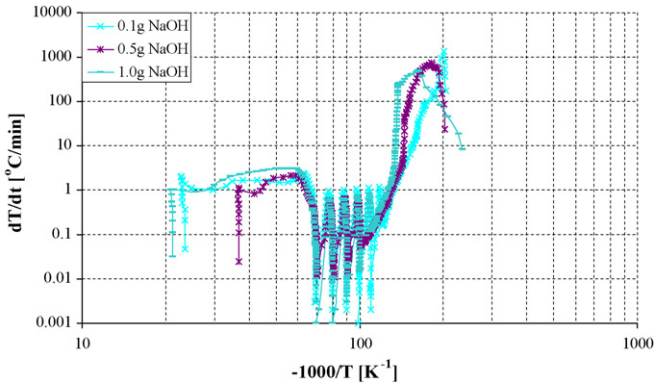

Fig. 14. Self-heat rate profiles of EO/NaOH samples.

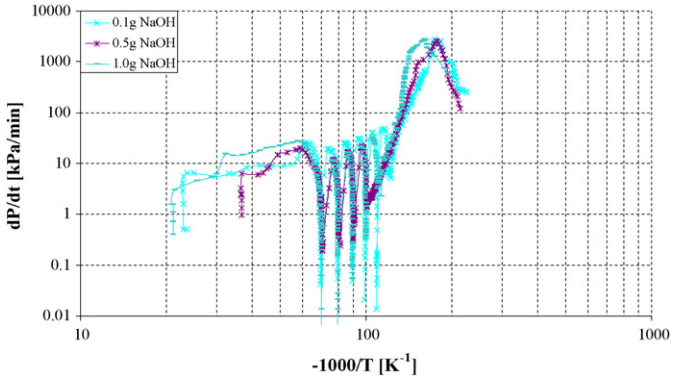

Fig. 15. Pressurization rate profiles of EO/NaOH samples.

able products. For the 0.5 g and 1.0 g tests, the cool-down pressure exceeds the heat up pressure.

For NaOH, the trends of the main parameters such as the onset temperature, maximum temperature, maximum heat rate, and maximum pressurization rate were difficult to see in Figs. 11–15. These trends are more clearly shown in the summary table (see Table 3). The onset temperature decreased by 15 °C when the NaOH concentration was increased 10 times from 0.1 g to 1.0 g. Also, the T_{max} were slightly decreased by an increase of the contaminant concentration. Meanwhile, two parameters including time to maximum heat rate and maximum pressurization rate were not really different and dT/dt_{max} was greatly reduced.

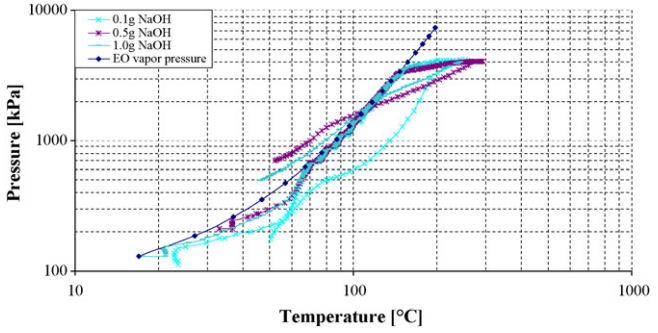

Fig. 16. Pressure–temperature profiles of EO/NaOH samples.

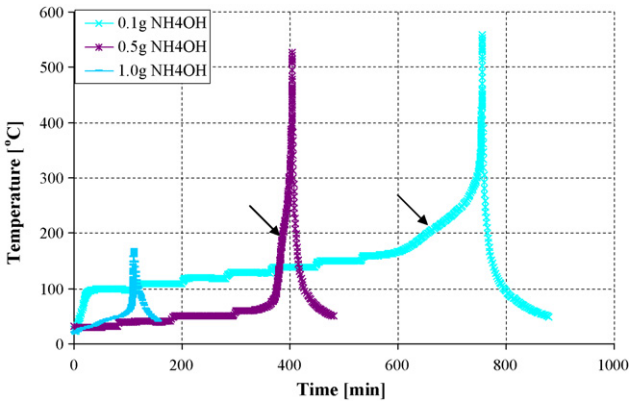

Fig. 17. Temperature history of EO/NH_4OH samples.

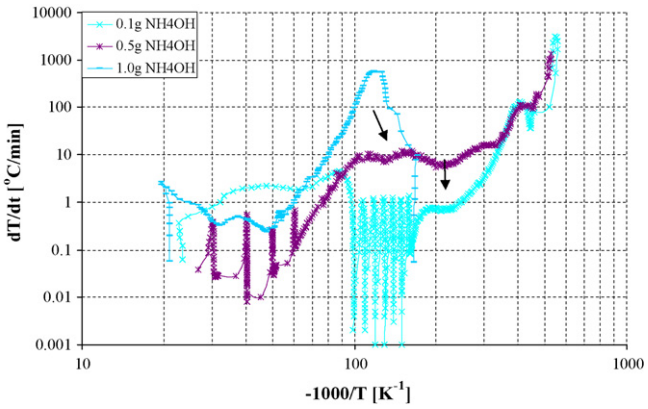

Fig. 18. Self-heat rate profiles of EO/NH_4OH samples.

3.4. Ethylene oxide in contact with ammonium hydroxide

Ammonium hydroxide solution was the third basic contaminant investigated in this research. Three amounts of ammonia, 0.1 g, 0.5 g, and 1.0 g from a 30% aqueous solution were added to 14 g of pure EO to examine their reactivity. Unlike the anhydrous hydroxide contaminants in the previous sections, this basic solution contained a highly volatile compound, NH_3, dissolved in water. In the presence of water, EO reacts with water to produce higher molecular weight glycols. The lowest observed onset temperature for neat EO with water in the absence of base was ~50 °C at 19% mass percent water [11]. However, onset temperatures with 5% mass percent water (1.0 g NH_4OH 30%) measured at ~21 °C were significantly lower than the 50 °C observed for the lowest measured onset temperature of EO contaminated by water alone. In short, it can be concluded that NH_4OH also reduces the onset temperature, and increases the maximum heat rate, and maximum pressurization rate of pure EO.

From Fig. 17, the EO mixtures with a higher NH_4OH concentration produced lower onset temperatures and lower maximum temperatures. For 0.1 g NH_4OH, the heat-wait-search continued until the mixture temperature reached about 160 °C. This relatively high onset temperature indicates that EO in contact with 0.7% mass of NH_4OH was relatively stable near ambient temperature. However, the onset temperature reduced quickly to 21 °C when the contaminant amount was increased 10 times to 1.0 g. Although the maximum temperature in the latter combination was much lower, this combination is more hazardous, because EO reacts significantly at ambient conditions.

Fig. 18 illustrates the self-heat rate profiles of EO/NH_4OH mixtures. For the case of 1.0 g NH_4OH, a self-heat rate of roughly

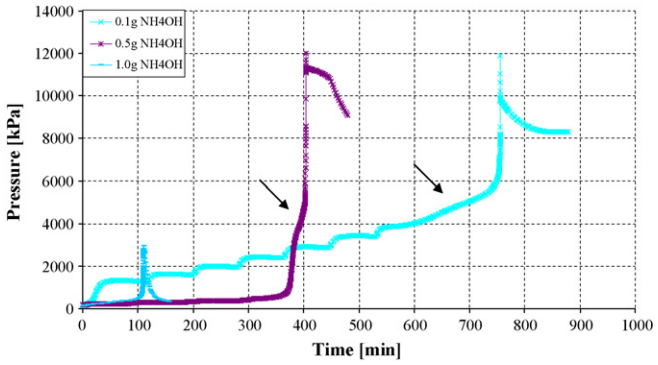

Fig. 19. Pressure history of EO/NH_4OH samples.

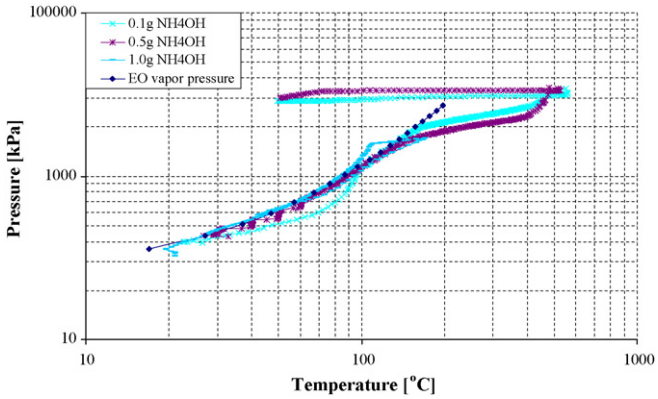

Fig. 21. Pressure–temperature profiles of EO/NH_4OH samples.

0.1 °C/min at near room temperature was observed, and acceleration to over 600 °C/min occurred within a short time thereafter. The 0.5 g NH_4OH/14 g EO samples showed a detectable exotherm at approximately 60 °C with the self-heating rate increased to nearly 10 °C/min around 100 °C. The self-heat rate remained nearly constant until about 280 °C and then began to accelerate yielding a self-heat rate up to 150 °C/min at 430 °C in the small peak. Subsequently, the rate dropped until the final stronger exotherm began at 450 °C and reached a higher peak of roughly 1300 °C/min. With a low concentration of NH_4OH (0.1 g), the maximum rate of heat generation of over 3000 °C/min was observed as well as the onset temperature up to 160 °C, which was much higher than those observed for 0.5 and 1.0 g NH_4OH.

Peak pressures of over 11721 kPa were generated in the cases of 0.1 g and 0.5 g NH_4OH (Fig. 19). For 1.0 g NH_4OH, the maximum pressure observed was ~2800 kPa.

As shown in Fig. 20, for 0.1 g and 0.5 g NH_4OH, the pressurization rate sudden increased at about 450 °C and reached over 20684 kPa/min which overwhelmed the pressure matching rate of the APTAC control system. As a result, the cells were ruptured or forced off the head of the containment vessel, following by the bursting of the containment vessel rupture disk near the end of these tests. The measured pressures at the peaks should be the ones in the containment vessel which may be lower the ones in an unbroken sample cell.

There is an unusual observation for this contaminant. There exists a small peak as a shoulder before the main peak. These peaks which were indicated with the arrows can be seen quite apparent in Figs. 17–19 for 0.1 g and 0.5 g NH_4OH. One possible explanation for these peaks can be as follows:

(1) First, the initial peaks may reflect the reaction between ammonia in the form of an aqueous solution and EO to produce ethanolamine with the water acting as a catalyst. As mentioned in the literature [17], the combination of EO and ammonia initially produces monoethyleneamine (MEA). However, because EO is extremely reactive, the secondary products, diethyleneamine (DEA) and triethyleneamine (TEA), are produced. All three reactions can occur within a short time and are highly exothermic [17].
(2) Because considerable energy is produced by the above reactions, an exotherm of EO took place, causing the ultimate peaks of increased sample temperature.

The pressures versus temperature plots in Fig. 21 also characterize pressure generation in the EO system. For the most part, the EO/NH_4OH samples followed the EO vapor pressure curve. At about 110 °C for 1.0 g NH_4OH and 150 °C for 0.1 g and 0.5 g NH_4OH, the pressures from these tests fall away from the EO vapor pressure curve, presumably because of EO consumption. Then, for 0.1 g and 0.5 g NH_4OH, the mixture pressures were still high despite the cooling period had ended because of increased nitrogen into the containment vessel following rupture of the titanium sample cells (Figs. 19 and 21).

Fig. 22 shows the EO/NH_4OH time to maximum heat rate, which is considerably longer than for KOH at a given temperature. In the presence of 0.1 g and 0.5 g NH_4OH, the mixture gave an explosion after 227 min near 571 °C and 102 min near 530 °C, respectively.

A summary of important parameters derived from the above figures are listed in Table 3. Compared to the two previous contaminants (KOH and NaOH), the key parameters for NH_4OH changed in much larger ranges when the amount of contaminant changed.

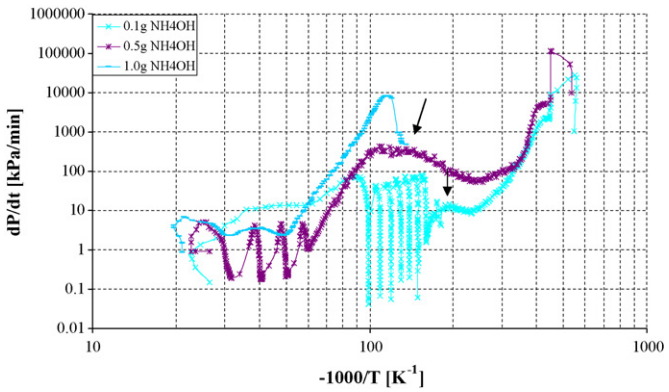

Fig. 20. Pressurization rate profiles of EO/NH_4OH samples.

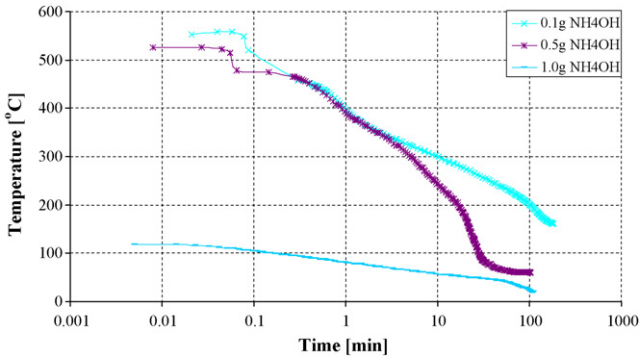

Fig. 22. Time-to-maximum profiles of EO/NH_4OH samples.

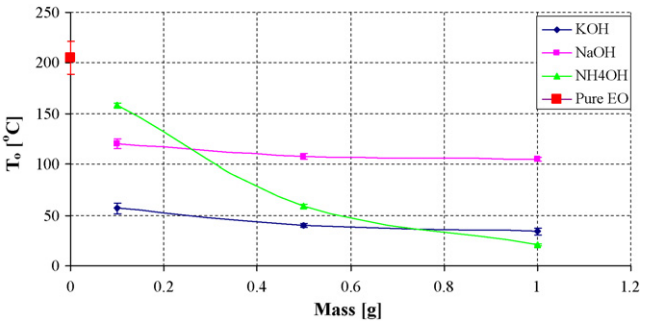

Fig. 23. Onset temperature–mass of contaminants profiles.

As can be seen in Table 3, T_{max}, P_{max}, dT/dt_{max}, and dP/dt_{max} decreased as the contaminant weight were increased, which are less hazardous trends. Only T_o and T_{MR} tends to more hazardous values.

3.5. Onset temperature comparison of ethylene oxide/contaminants

The onset temperature is an important parameter for evaluation of the contamination effects on EO thermal stability. Fig. 23 displays the onset temperatures of different contaminants and different contaminant concentrations to illustrate the impact of contaminant concentration on the measured exothermic onset temperatures more clearly. The T_o values in Fig. 17 are the average values from the test results. The detected onset temperature increases as the contaminant mass is decreased and does not exceed the value measured for pure EO. This figure clearly shows that the stability of EO is strongly affected by the KOH. The onset temperature of pure EO is reduced from ~205 °C to ~60 °C or below even with a small amount of KOH (0.1 g). Over the same investigated range of contaminant concentration, the onset temperatures of NaOH and KOH were slightly reduced to lower values at higher contaminant concentrations, while the ones for NH_4OH were dramatically reduced.

Fig. 23 also shows that the behavior of the NaOH appears to parallel that of the KOH except for being displaced to higher onset temperatures by 60–70 °C. KOH and NaOH have similar structures and properties, but their effects on EO behavior are quite different.

4. Conclusions

Evaluation of EO reactivity in contact with three industrial contaminants, KOH, NaOH, and NH_4OH was performed with measurements using an APTAC. Small amounts (0.1 g, 0.5 g, and 1.0 g) of these chemical compounds were mixed with 14 g EO and heated to measure the EO exothermic reaction behavior catalyzed by the contaminants.

The 14 g of pure EO required about 205 °C to initiate runaway reaction under adiabatic conditions and produced a maximum temperature of about 600 °C and pressure of approximately 11790 kPa in a 130 mL sample cell. The tested contaminants affected measured values of these parameters. All greatly exhibited catalytic effects on the reactivity of EO and caused reductions in the runaway reaction threshold temperatures.

In the studied range of contaminant concentrations, T_o, dT/dt_{max}, dP/dt_{max} and T_{MR} changed to more hazardous values when the amount of KOH increased. With each of NaOH and NH_4OH, the contaminated EO underwent exotherm reactions at lower and more hazardous values of T_o and T_{MR}.

At the same levels of 0.1 g, 0.5 g, and 1.0 g contaminant, the contaminants all lowered the EO onset temperature but different effects. With 1.0 g, NaOH reduced the onset temperature to around 100 °C while KOH and NH_4OH decreased it to room temperature. Especially, KOH can initiate an exotherm roughly 60 °C even at low concentration (0.1 g KOH/14 g EO).

Among the investigated contaminants, the presence of NH_4OH with a sufficient concentration has the highest impact on T_{max}, P_{max}, dT/dt_{max}, and dP/dt_{max} of contaminated EO. By 59 °C, the combinations of EO and 0.5 g NH_4OH (~3.5 wt.%) was reached the maximum self-heat rate near 530 °C after 102 min. The following relative reactivity of contamination is suggested: NH_4OH > KOH > NaOH.

To be of greater use, the thermokinetics of the reactions of EO with KOH, NaOH, and NH_4OH should be determined in future work. Additional experiments over wider ranges of phi-factor and EO mass fraction as well as product identification should be made for a thorough kinetics understanding and development of kinetic models for these reactions. With additional experimental data and kinetics models, simulation models can be developed to reproduce APTAC measured data and predict scaled-up onset temperature, time to maximum rate, and maximum pressure for ranges of EO volume, concentration, and operation conditions. Increased information and modeling of EO behavior can aid safety-related decisions regarding processing, storage, handling, stable conditions, emergency relief system design, and incident investigations. In addition, this information will be valuable in guiding implementation of inherently safer process designs and technology for EO applications.

References

[1] C. Buckles, P. Chipman, M. Cubillas, M. Lakin, D. Slezak, D. Townsend, K. Vogel, M. Wagner, Ethylene oxide user's guide, second ed., http://www.ethyleneoxide.com. 1999. Accessed August 07, 2007.
[2] NIOSH, EPA, EOSA, Preventing worker injuries and deaths from explosions in industrial ethylene oxide sterilization facilities. http://www.epa.gov/oem/docs/chem/etoalert.pdf. Accessed September 16, 2008.
[3] G. Viera, L.L. Simpson, B.C. Ream, Chem. Eng. Prog. 89 (1993) 66–75.
[4] R.G. Vanderwater, Chem. Eng. Prog. 85 (1989) 16–20.
[5] J. Woodward, J.W. Wesevich, J.K. Thomas, Q.A. Baker, Proc. Saf. Prog. 26 (2) (2007) 150–154, June.
[6] T.A. Kletz, Plant/Oper. Prog. 7 (1988) 226–230.
[7] J.E. Troyan, R.Y. LeVine, AlChE Loss Prev. 2 (1968) 125–130.
[8] L. Bretherick, P.G. Urben, Bretherick's Handbook of Reactive Chemical Hazards, 5th ed., Butterworth–Heinemann, 1995.
[9] L.G. Britton, Plant/Oper. Prog. 9 (1990) 75–86.
[10] M.E. Levin, J. Hazard. Mater. 104 (2003) 227–245.
[11] G.A. Melhem, M.E. Levin, H.G. Fisher, S. Chippelt, S.K. Singh, P.L. Chipman, Proc. Saf. Prog. 20 (2001) 231–246.
[12] S. Freeder, T.J. Snee, J. Loss Prev. Proc. 1 (1988) 164–168.
[13] S. Chippett, P. Ralbovsky, R. Granville, Proceedings of the International Symposium on Runaway Reaction Pressure Relief Design and Effluent Handling, 1998, pp. 81–108.
[14] E. Wilcock, R. Rogers, J. Loss Prev. Proc. Ind. 10 (1997) 289–302.
[15] http://www.cheric.org/kdb/kdb/hcprop/showprop.php?cmpid=1042. Retrieved on July 10, 2008.
[16] Efunda. http://www.efunda.com/materials/elements/HC_Table.cfm?Element_ID=Ti. Accessed March 20, 2008.
[17] Patent storm. http://www.patentstorm.us/patents/5545757-description.html: Production of ethanolamines. Accessed March 20, 2008.